

# Physics with Identified Particles at STAR

**Lijuan Ruan (for the STAR Collaboration<sup>†</sup>)**

Nuclear Science Division, MS 70R319, Lawrence Berkeley National Lab, Berkeley,  
CA 94720

E-mail: [ljruan@lbl.gov](mailto:ljruan@lbl.gov)

**Abstract.** New physics results with identified particles at STAR are presented. Measurements at low  $p_T$  address bulk properties of the collision, while those at high  $p_T$  address jet energy loss in the bulk matter produced. Between these extremes, measurements at intermediate  $p_T$  address the interplay between jets and the bulk. We highlight: measurements of  $v_2$  fluctuations as a new, sensitive probe of the initial conditions and the equation of state; correlations involving multi-strange particles, along with ratios of identified particles to test coalescence as a mechanism of particle production at intermediate  $p_T$ ; three particle azimuthal correlation to search for conical emission; and the energy and particle-type dependence of hadron production at high  $p_T$  to study quark and gluon jet energy loss.

## 1. Introduction

Comparisons between experiment and theory suggest that central Au+Au collisions at RHIC produce dense and rapidly thermalizing matter characterized by initial energy densities far above the critical values predicted by lattice QCD for formation of a Quark-Gluon Plasma, accompanied by nearly ideal fluid flow, marked by constituent interactions of very short mean free path, established most probably at a stage preceding hadron formation, along with opacity to jets [1]. In order to study the properties of the partonic matter created in Au+Au collisions in detail, we would like to address the following physics topics using the data taken by the STAR experiment at RHIC:

Bulk properties and Equation of State (EOS) by using anisotropic flow at low  $p_T$  ( $p_T < 2$  GeV/c), energy dependences of fluctuations and freeze-out properties, and intermediate and low  $p_T$  charged hadron azimuthal correlations.

Coalescence/recombination at intermediate  $p_T$  ( $2 < p_T < 6$  GeV/c) by using identified baryon and meson  $v_2$ , baryon and charged hadron azimuthal correlations, and energy dependence of particle production.

Parton energy loss in the medium by using identified particle spectra at high  $p_T$  ( $p_T > 6$  GeV/c).

<sup>†</sup> For the full author list and acknowledgements see Appendix “Collaborations” in this volume.

## 2. Equation of State

### 2.1. Anisotropic Flow $v_1$ , $v_2$ and $v_2$ Fluctuation

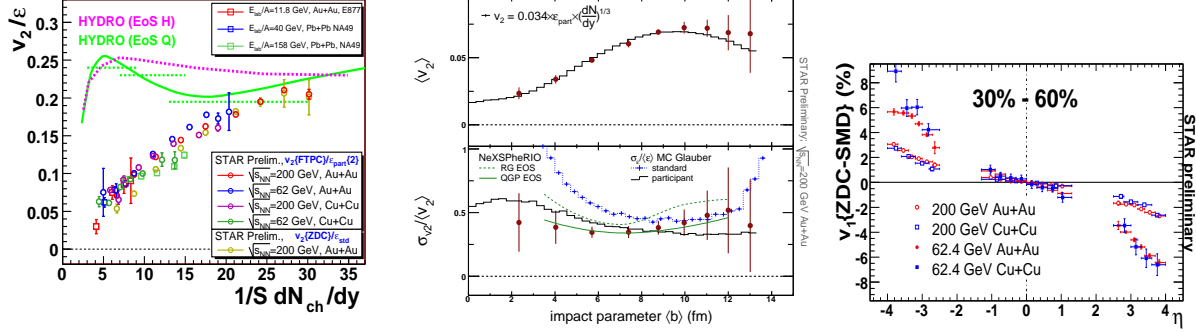


**Figure 1.** (in color on line) (left) The  $v_2/\epsilon$  versus  $\frac{1}{S}dN_{ch}/dy$ . (middle) The  $\langle v_2 \rangle$  and  $\sigma_{v_2}/\langle v_2 \rangle$  versus  $\langle b \rangle$  in Au+Au collisions at 200 GeV. (right)  $v_1$  versus pseudo-rapidity  $\eta$ .

The large elliptic flow ( $v_2$ ) observed at RHIC is sensitive to pressure gradients developed in the early stages of heavy ion collisions, and so is believed to be sensitive to the EOS. Further insight into the processes governing the evolution of the system, and the physics underlying the formation of the flow itself, can be provided by the study of its dependence on system size and collision energy. Fig. 1 (left) shows the ratio of integral  $v_2$  over the spatial eccentricity ( $\epsilon$ ) as a function of charged particle density in the transverse plane ( $\frac{1}{S}dN_{ch}/dy$ ) from Au+Au and Cu+Cu collisions at  $\sqrt{s_{NN}} = 62$  and 200 GeV [2], where  $S$  is the overlap area in the transverse plane weighted with the number of participants along the beam axis [3]. In this plot,  $v_2\{FTPC\}$  is derived via correlations between a particle in the main TPC and those in the Forward TPC [2], reducing non-flow effects, while  $v_2\{ZDC\}$  is derived using the reaction plane from the STAR ZDC-SMD. After  $v_2\{FTPC\}$  and  $v_2\{ZDC\}$  are scaled with appropriate values of eccentricity [2], a universal curve of  $v_2/\epsilon$  versus  $\frac{1}{S}dN_{ch}/dy$  is observed for all the energy and collision systems. The  $v_2/\epsilon$  value in central Au+Au collisions reaches the hydrodynamic limit with QGP EOS, suggesting possible thermalization achieved in central Au+Au collisions.

The first  $v_2$  fluctuation measurement at STAR allows us to remove the major source of systematic uncertainty for  $\langle v_2 \rangle$  and provides sensitivity to initial conditions [4]. Fig. 1 (middle) shows, as a function of impact parameter ( $\langle b \rangle$ ), both the mean  $v_2$  ( $\langle v_2 \rangle$ ) (upper panel) and a measure of the event-by-event fluctuations of  $v_2$ , the r.m.s. over the mean ( $\sigma_{v_2}/\langle v_2 \rangle$ ) (lower panel). The fluctuation measure is found to be  $\sim 36\%$ , approximately independent of centrality, which corresponds well with the fluctuations in initial-state eccentricity derived in a Glauber model [4]. Comparisons with hydrodynamic models indicate further that the fluctuations may be sensitive to the EOS. The dependence of directed flow ( $v_1$ ) on system size is strikingly different from that of  $v_2$ . While  $v_2$  appears to scale with the transverse particle density,  $v_1$  appears to scale with the fraction of

the hadronic cross-section measured. Fig. 1 (right) shows that, while  $v_1$  has a strong dependence on collision energy, for the same fraction of the hadronic cross-section, e.g. collisions with 30-60% centrality,  $v_1$  is similar in Cu+Cu and Au+Au collisions [5].

## 2.2. Two and Three Particle Correlations — Medium Responses to Jet Energy Loss

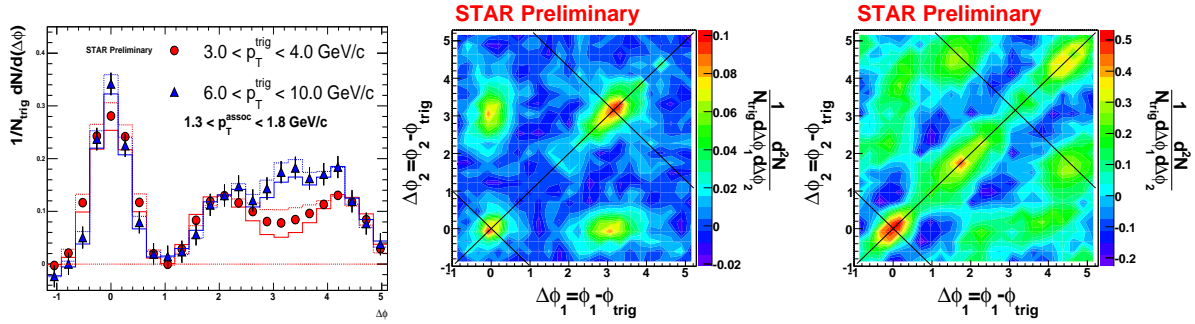


**Figure 2.** (in color on line) (left) Two particle azimuthal correlations in 0-12% central Au+Au collisions after background subtraction. (middle and right) Three particle azimuthal correlations after background subtraction in 200 GeV d+Au and 0-12% central Au+Au collisions respectively with a trigger particle at  $3 < p_T^{\text{trig}} < 4$  GeV/c and two associated particles at  $1 < p_T^{\text{asso}} < 2$  GeV/c.

The comparison of the measurement of elliptic flow and its calculated value from hydrodynamic models indicates early thermalization in central Au+Au collisions. If this is true, the next question is how the system achieves thermalization. In correlations between particles at high  $p_T$  (hard) and those at low  $p_T$  (soft), the mean  $p_T$  of soft particles on the away-side from the hard trigger particle approaches that of the bulk soft particles in central Au+Au collisions [6], indicating that hard-soft interactions lead to partial thermalization. One proposed mechanism for rapid thermalization between the deposited energy and the bulk medium is through Mach-cone shock waves, which disperse energy into collective modes [7, 8]. Fig. 2 (left) shows the di-hadron azimuthal correlations in central Au+Au collisions for a fixed associated  $p_T$  range and two selections of trigger  $p_T$  ( $p_T^{\text{trig}}$ ) ranges [9]. The away-side structure strongly depends on  $p_T^{\text{trig}}$ . And a double peaked structure on the away-side is observed for the lower  $p_T^{\text{trig}}$  range. This structure can be generated by several physics mechanisms including Mach-cone shock waves [7, 8], deflected jets, and Čerenkov radiation [10].

In order to distinguish and/or further separate the contributions from different physics scenarios, event-by-event three particle correlations are measured at STAR using two analysis approaches: the cumulant method, and background-subtraction method. The results from the cumulant method show unambiguous evidence for three particle correlations [11]. In order to interpret the signal, the background-subtraction method, using a model treating the event as the sum of correlated particles and an uncorrelated background (with flow anisotropy), is applied [11, 12]. Fig. 2 (middle) and (right) show three particle correlations from the background subtraction method in d+Au and central Au+Au collisions after background subtraction [11, 12]. In these

plots, the deflected jet effect will lead to the on-diagonal structure and Mach-cone shock waves/Čerenkov radiation will lead to additional off-diagonal structure. In d+Au collisions, clear near-side and away-side jet structures are observed. In central Au+Au collisions, in addition to those, on-diagonal and off-diagonal structures are observed. The on-diagonal structure is consistent with the deflected jet scenario. The off-diagonal one shows evidence for conical emission. Whether it is due to Mach-cone or gluon Čerenkov radiation needs more detailed quantitative comparison with theoretical models and measurements with identified particles, different beam energy, as well as associated  $p_T$  dependence, preliminary results of which are presented at this conference by STAR [12].

### 2.3. Bulk Properties in Energy Scan

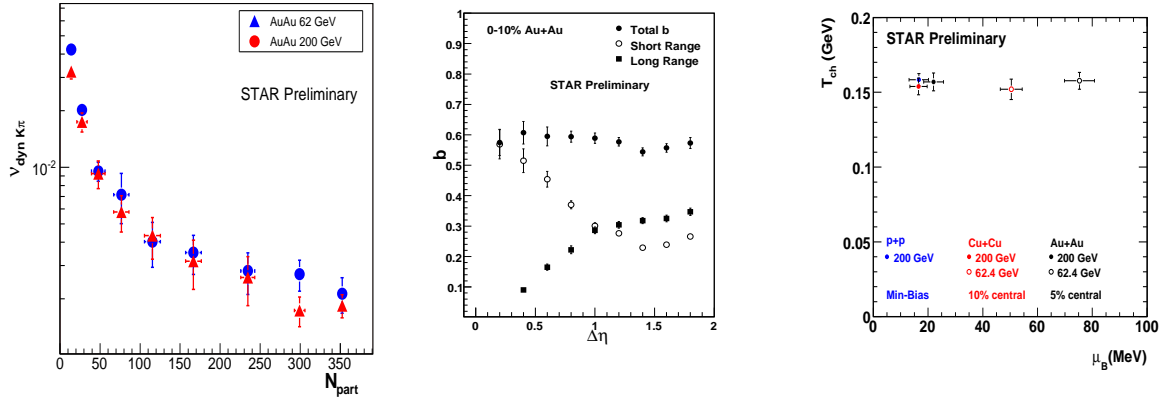


**Figure 3.** (in color on line) (left) The  $v_{dyn} K\pi$  fluctuation versus centrality. (middle) The long range and short range correlation strength versus pseudo-rapidity gap. (right)  $T_{ch}$  versus  $\mu_B$ .

Fig. 3 (left) shows that the dynamical fluctuations in  $K/\pi$  ratio ( $v_{dyn} K\pi$  [13]) are similar in Au+Au collisions at 62 and 200 GeV [13]. Fig. 3 (middle) shows the correlation strength ( $b$ ) and its long and short range components, versus pseudo-rapidity gap ( $\eta_{gap}$ ) in central Au+Au collisions [14]. The growth of long range  $\Delta\eta$  correlations is clearly seen, the existence of which is the signature of multiple parton inelastic collisions and hence possible creation of dense partonic matter [15]. Fig. 3 (right) shows the chemical freeze-out temperature ( $T_{ch}$ ) versus baryon chemical potential ( $\mu_B$ ) derived from the thermal fit to  $\pi, K$  and  $p$  spectra [16]. With decreasing beam energy, the baryon chemical potential increases. In the QCD phase diagram, the critical point, namely the end point of the first order phase transition, is predicted to be at  $350 < \mu_B < 700$  MeV from Lattice QCD calculations [17]. This value is significantly larger than the  $\mu_B$  value at which matter is formed in RHIC collisions in energies scanned to date. In a future energy scan to lower energy, matter will be formed in the relevant region in  $\mu_B$ , allowing for a search for the critical point using systematic measurements of fluctuations and spectra of identified particles.

### 3. Coalescence

#### 3.1. Number of Constituent Quark (NCQ) Scaling of $v_2$

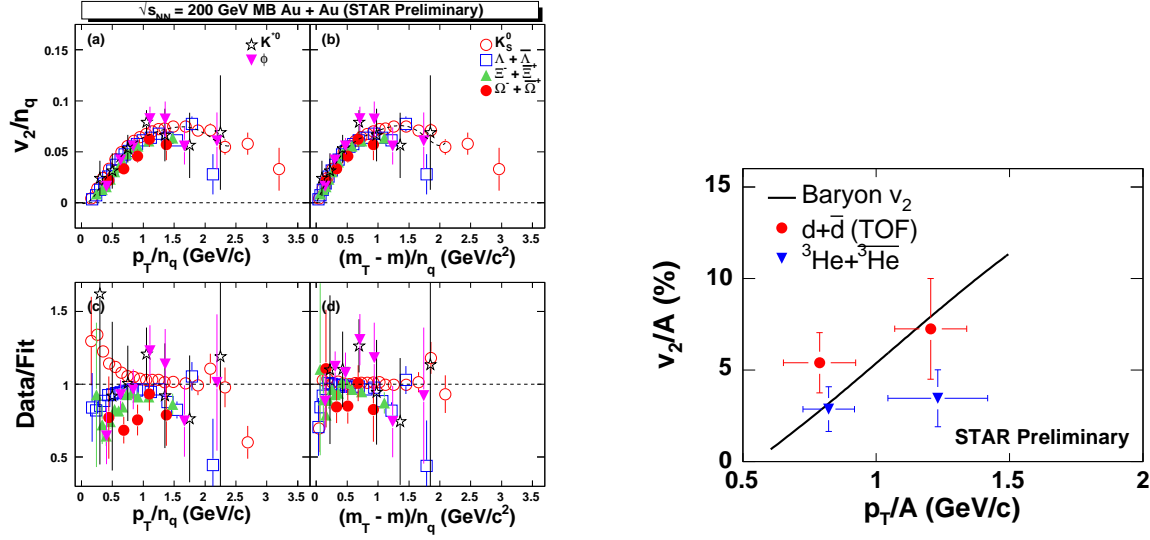


**Figure 4.** (in color on line) (left) Identified baryon and meson  $v_2/n_q$  versus  $p_T/n_q$  or  $(m_T - m_0)/n_q$ . (right) The atomic mass number ( $A$ ) scaled  $v_2$  of light nuclei versus  $p_T/A$ .

Fig. 4 (left) shows  $v_2$  divided by the number of constituent quarks ( $n_q$ ) versus  $p_T/n_q$  or  $(m_T - m_0)/n_q$  of  $K_S^0$ ,  $\Lambda$ ,  $\Xi$ ,  $\Omega$ ,  $K^*$  and  $\phi$  [18, 19, 20]. A common fit to all the data points was used and the ratios of the data points over the common fit function are shown in the lower panel. At low  $p_T$ ,  $v_2$  shows strong mass ordering, consistent with hydrodynamical models [21]. At intermediate  $p_T$ ,  $v_2$  of mesons ( $K_S^0$ ,  $K^*$ ,  $\phi$ ) and baryons ( $\Lambda$ ,  $\Xi$ ,  $\Omega$ ) follow NCQ scaling, consistent with hadronization through coalescence of constituent quarks from a collective partonic system [22, 23, 24, 25]. Light nuclei, such as the deuteron and  ${}^3\text{He}$ , can be formed by coalescence at the nucleon level when interactions between nucleons and other particles are weak. The  $v_2$  measurements of nuclei can be used to test the general feature of coalescence. Fig. 4 (right) shows  $v_2$  of deuteron and  ${}^3\text{He}$  divided by atomic mass number ( $A$ ) as a function of  $p_T/A$  [26]. The deuteron  $v_2$  seems to follow  $A$  scaling while  ${}^3\text{He}$  shows a possible deviation at the higher  $p_T$  bin.

#### 3.2. Multi-Strange Particle Production and Correlations

To further understand the particle production mechanisms and test the coalescence model predictions, we measure the correlations between strange and multi-strange baryons and charged hadrons. Shown in Fig. 5 (left) is the azimuthal correlation of two particles with a baryon ( $\Lambda$ ,  $\Xi$ , or  $\Omega$ ) trigger, and an associated charged hadron ( $h$ ) [27]. The  $\Lambda$ ,  $\Xi$ , or  $\Omega$  -  $h$  correlations are similar, and a strong near-side correlation of  $\Omega$  -  $h$  is observed. This is in contrast to the recombination model [28], which predicts no near-side particle to be associated with a multi-strange  $\Omega$  or  $\phi$  trigger. In this

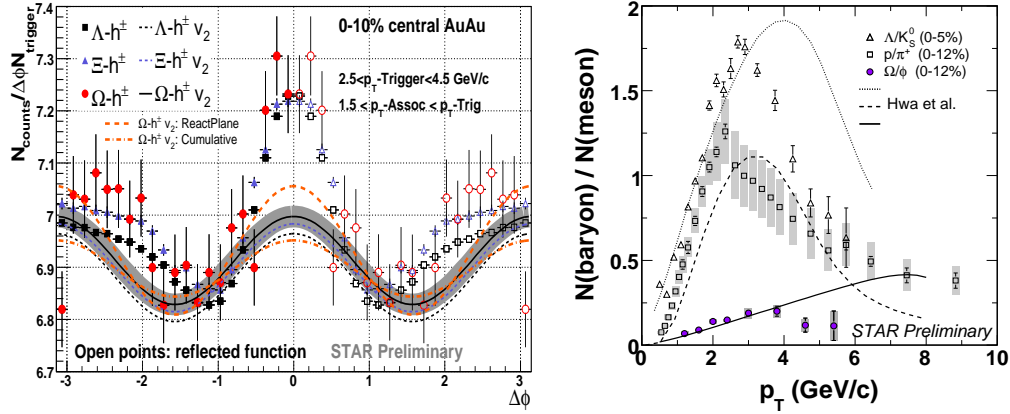


**Figure 5.** (in color on line) (left) The baryon and charged hadron azimuthal correlations in central Au+Au collisions at 200 GeV. (right) The baryon over meson ratios in central Au+Au collisions at 200 GeV.

model, the multi-strange particles ( $\Omega(sss)$  and  $\phi(s\bar{s})$ ) mainly come from thermal s quark recombination.

Fig. 5 (right) shows the  $\Omega/\phi$ ,  $\Lambda/K_S^0$  and  $p/\pi^+$  ratios versus  $p_T$  in 200 GeV central Au+Au collisions [19], compared with the calculations from a recombination model [23, 28]. The  $\Omega/\phi$  ratio increases as a function of  $p_T$ , reaches its maximum value at  $p_T \sim 4$  GeV/c, then shows a decreasing trend at higher  $p_T$ . The recombination model [28] can describe the  $\Omega/\phi$  ratio up to  $p_T \sim 4$  GeV/c but fails to reproduce the ratio at higher  $p_T$ , indicating non-thermal s quark contribution to the  $\phi$  and  $\Omega$  production in this  $p_T$  region.

### 3.3. Energy Dependence of Identified Particle Production at Intermediate/High $p_T$

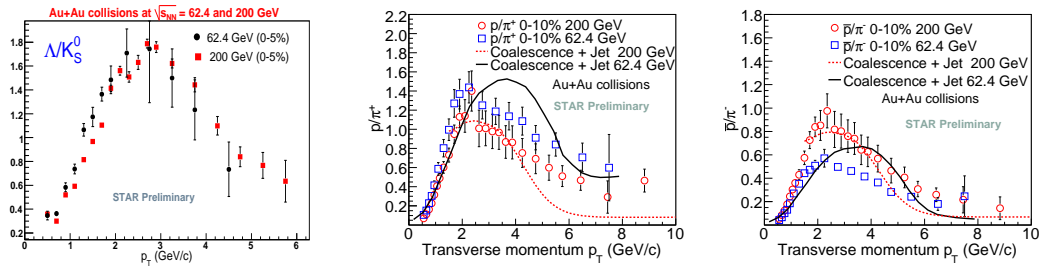


**Figure 6.** (in color on line) The  $\Lambda/K_S^0$ ,  $p/\pi^+$  and  $\bar{p}/\pi^-$  ratios in central Au+Au collisions at 62 and 200 GeV.

The energy dependence of identified particle production provides a tool to further test the coalescence and jet quenching [29]. Coalescence models predict a higher(lower)  $p/\pi^+$  ( $\bar{p}/\pi^-$ ) ratio at 62 GeV compared to 200 GeV at intermediate  $p_T$  [25]. Fig. 6 shows the  $\Lambda/K_S^0$ ,  $p/\pi^+$  and  $\bar{p}/\pi^-$  ratios as a function of  $p_T$  in central Au+Au collisions at 62 and 200 GeV [30]. At intermediate  $p_T$ , we observe:  $p/\pi^+(62 \text{ GeV}) > p/\pi^+(200 \text{ GeV})$

GeV);  $\Lambda/K_S^0$  (62 GeV)  $\sim \Lambda/K_S^0$  (200 GeV) and  $\bar{p}/\pi^-(62 \text{ GeV}) < \bar{p}/\pi^-(200 \text{ GeV})$ . Furthermore, we find the  $\Lambda/K_S^0$ ,  $p/\pi^+$  and  $\bar{p}/\pi^-$  ratios show similar peak positions and similar shapes at these two energies. Also shown are the calculations from coalescence + jet fragmentation models [24, 25]. At intermediate  $p_T$ , the calculations can reproduce the  $p/\pi^+$  and  $\bar{p}/\pi^-$  ratios at 200 GeV but can not reproduce the ratios at 62 GeV. Compared to the data, the peak positions of the ratios from model are shifted to higher  $p_T$  with energy decreasing. In general, at high  $p_T$ , jet fragmentation models [24, 25] can not reproduce the particle ratios.

#### 4. Study of Parton Energy Loss by Identified Baryon/Meson at High $p_T$

At  $p_T > 6 \text{ GeV}/c$ , particle production is dominated by jet fragmentation in Au+Au collisions. Identified particles at high  $p_T$  provide direct sensitivity to differences between quark and gluon fragmentation. For example, the gluon contribution to  $\pi^+ + \pi^-$  is around 50% while that to  $p + \bar{p}$  is larger than 80% at  $6 < p_T < 10 \text{ GeV}/c$  in 200 GeV p+p collisions [31, 32]. The Casimir/color factors ( $C_A$ ,  $C_F$ ) of gluon and quark

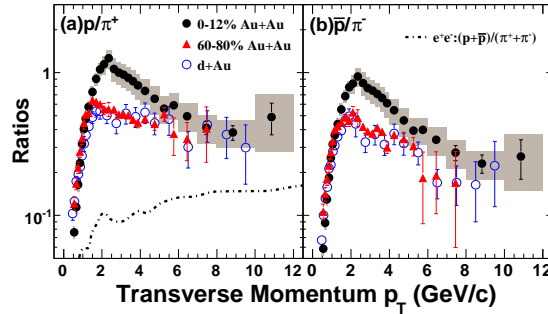


**Figure 7.** (in color on line) The  $p/\pi^+$  and  $\bar{p}/\pi^-$  ratios in d+Au [32] and Au+Au collisions [33].

have been determined in elementary  $e^+ + e^-$  collisions [34]. It's found that  $C_A/C_F$ , the ratio of the coupling strength of the triple-gluon vertex to that of gluon bremsstrahlung from quarks is  $\sim 2$ , which is in agreement with the value expected from SU(3) QCD theory [34]. When traversing the hot and dense medium created in the collisions, gluons lose more energy than quarks [29, 35, 36]. Therefore, the  $\bar{p}/\pi$  ratio in central Au+Au collisions is expected to be smaller than those in peripheral Au+Au, d+Au and p+p collisions [36]. Fig. 7 shows that the  $\bar{p}/\pi^-(p/\pi^+)$  ratios in central Au+Au [33] and d+Au [32] collisions are similar at  $p_T > 5 \text{ GeV}/c$ . This common degree of suppression of protons and pions indicates that the partonic sources of pions and protons have similar energy loss, which can not be explained by simple color factor differences [36]. One possible solution is to consider additional processes in the interaction of jets with the medium. For example, recently, the jet conversion in the medium is considered and it is found that in order to reproduce the data, a jet conversion rate much larger than expected may be needed [37].



## 5. Summary

In summary, we have presented a wealth of measurements from STAR to study the properties of the partonic medium.

A common degree of suppression of protons and pions at high  $p_T$  is observed. This new experimental phenomenon provides strong constraints on the interaction of jets with the medium. The interaction of jets with the medium leads to double peaked structure on the away-side in di-hadron azimuthal correlations in selected kinematic regions. The three particle correlations, in the background-subtraction method, show evidence for conical emission.

In the bulk, constituent interactions at the early stage transfer the spatial anisotropy into significant momentum anisotropy in the transverse plane. Significant fluctuations in  $v_2$  have been observed, which coincide with fluctuations in the initial eccentricity.  $v_2$  of identified particle  $K_S^0$ ,  $\Lambda$ ,  $\Xi$ ,  $\Omega$ ,  $K^*$  and  $\phi$  at intermediate  $p_T$  show constituent quark number scaling, consistent with hadronization through coalescence of constituent quarks from a collective partonic system.

However, at intermediate  $p_T$ , there are several differences observed between coalescence/recombination models and data. The  $p(\bar{p})/\pi$  ratios show similar peak positions at 62 and 200 GeV. A strong near-side correlation of  $\Omega - h$  is observed and the  $\Omega/\phi$  ratio turns over at  $p_T \sim 4$  GeV/c. These observations need further theoretical exploration [38].

## References

- [1] J. Adams *et al.* (STAR Collaboration), Nucl. Phys. A **757**, 102 (2005).
- [2] S. Voloshin *et al.* (STAR Collaboration), these proceedings and references therein.
- [3] S. Voloshin and A. Poskanzer, Phys. Lett. B **474**, 27 (2000).
- [4] P. Sorensen *et al.* (STAR Collaboration), these proceedings and references therein, nucl-ex/0612021.
- [5] G. Wang *et al.* (STAR Collaboration), these proceedings.
- [6] J. Adams *et al.*, Phys. Rev. Lett. **95**, 152301 (2005).
- [7] H. Stoecker, Nucl. Phys. A **750**, 121 (2005).
- [8] J. Casalderrey-Solana, E.V. Shuryak and D. Teaney, J. Phys. Conf. Ser. **27**, 22 (2005).
- [9] M. Horner *et al.* (STAR Collaboration), these proceedings.
- [10] A. Majumder *et al.*, Phys. Rev. C **73**, 051901 (2006); V. Koch *et al.*, Phys. Rev. Lett. **96**, 172302 (2006).
- [11] C. Pruneau *et al.* (STAR Collaboration), these proceedings.
- [12] J. Ulery *et al.* (STAR Collaboration), these posters.
- [13] S. Das *et al.* (STAR Collaboration), these posters.
- [14] B. Srivastava *et al.* (STAR Collaboration), these posters.
- [15] A. Capella *et al.*, Phys. Rep. **236**, 225 (1994).
- [16] A. Iordanova *et al.* (STAR Collaboration), these posters.
- [17] Z. Fodor *et al.*, JHEP **0404**, 050 (2004); Phys. Lett. B **534**, 87 (2002); JHEP **0203**, 014 (2002).
- [18] Y. Bai *et al.* (STAR Collaboration), these proceedings.
- [19] S. Blyth *et al.* (STAR Collaboration), these proceedings and references therein.
- [20] X. Dong *et al.* (STAR Collaboration), these posters.
- [21] D. Teaney *et al.*, nucl-th/0110037; D. Teaney *et al.*, Phys. Rev. Lett. **86**, 4783 (2001); P. Huovinen, Nucl. Phys. A **715**, 299c (2003); P. Kolb *et al.*, Phys. Rev. C **67**, 044903 (2003).



- [22] D. Molnar *et al.*, Phys. Rev. Lett. **91**, 092301 (2003).
- [23] R.C. Hwa *et al.*, Phys. Rev. C **70**, 024905 (2004).
- [24] R.J. Fries *et al.*, Phys. Rev. C **68**, 044902 (2003).
- [25] V. Greco *et al.*, Phys. Rev. Lett. **90**, 202302 (2003); Phys. Rev. C **71**, 041901 (2005).
- [26] H. Liu *et al.* (STAR Collaboration), these proceedings and references therein.
- [27] J. Bielcikova *et al.* (STAR Collaboration), these proceedings.
- [28] R. Hwa *et al.*, nucl-ex/0602024.
- [29] M. Gyulassy *et al.*, nucl-th/0302077; A. Kovner *et al.*, hep-ph/0304151.
- [30] B. Mohanty *et al.* (STAR Collaboration), these proceedings.
- [31] S. Albino *et al.*, Nucl. Phys. B **725**, 181 (2005).
- [32] J. Adams *et al.*, Phys. Lett. B **616**, 8 (2005); J. Adams *et al.*, Phys. Lett. B **637**, 161 (2006).
- [33] B.I. Abelev *et al.*, Phys. Rev. Lett. **97**, 152301 (2006).
- [34] P. Abreu *et al.*, Z. Phys. C **59**, 357 (1993).
- [35] J. Adams *et al.*, Phys. Rev. Lett. **91**, 172302 (2003).
- [36] X.N. Wang, Phys. Rev. C **58**, 2321 (1998); Q. Wang *et al.*, Phys. Rev. C **71**, 014903 (2005).
- [37] W. Liu *et al.*, nucl-th/0607047.
- [38] R. Hwa, these proceedings, nucl-th/0701018.